

Untangling the merger history of massive black holes with *LISA*

Scott A. Hughes*

Institute for Theoretical Physics, University of California, Santa Barbara CA 93106, USA

1 June 2021

ABSTRACT

Binary black hole coalescences emit gravitational waves that will be measurable by the space-based detector *LISA* to large redshifts. This suggests that *LISA* may be able to observe black holes grow and evolve as the universe evolves, mapping the distribution of black hole masses as a function of redshift. An immediate difficulty with this idea is that *LISA* measures certain *redshifted* combinations of masses with good accuracy: if a system has some mass parameter m , then *LISA* measures $(1+z)m$. This mass-redshift degeneracy makes it difficult to follow the mass evolution. In many cases, *LISA* will also measure the luminosity distance D of a coalescence accurately. Since cosmological parameters (particularly the mean density, the cosmological constant, and the Hubble constant) are now known with moderate precision, we can obtain z from D and break the degeneracy. This makes it possible to untangle the mass and redshift and to study the mass and merger history of black holes. Mapping the black hole mass distribution could open a window onto an early epoch of structure formation.

Key words: gravitational waves – gravitation – black hole physics – cosmology: miscellaneous

1 INTRODUCTION

Evidence from quasars at redshifts $z > 5$ makes it clear that massive black holes have existed since the universe’s youth (Stern et al. 2000; Zheng et al. 2000; Fan et al. 2000). In order to be powering quasars at $z \sim 5$, seed black holes with masses of $10^5 M_\odot$ or so had to exist at $z \sim 10$ (Gnedin 2001). In hierarchical formation scenarios, these seed holes are produced by the infall and merger of baryonic and dark matter clumps, and are then associated with dark matter halos. As the halos interact and merge to form larger structures and eventually galaxies, the black holes that they contain can merge as well [although there may be many more halo and structure mergers than there are black hole mergers; see Milosavljević & Merritt (2001)]. This creates a population of coalescing massive black holes at cosmological distances.

These coalescing black holes will be strong sources of gravitational radiation. It has been known for some time that such coalescences will be detectable by the space-based gravitational-wave antenna *LISA* (Thorne 1995; Haehnelt 1998; Flanagan & Hughes 1998). This suggests that *LISA* could be used to map the distribution of black holes as the universe evolves, tracing the growth and evolution of the massive black hole population. Such observations could shed light on the merger of the black hole’s host structures, pro-

viding information about the development of structure in the universe (Menou, Haiman, & Narayanan 2001).

By tracking the gravitational-wave phase as the black holes inspiral and merge, *LISA* accurately measures certain mass parameters of the binary system. Unfortunately, the masses that *LISA* will measure are redshifted. Modulo overall amplitude, the gravitational waves that we measure from a binary with masses $[m_1, m_2]$ at redshift z are those of a local binary with masses $[(1+z)m_1, (1+z)m_2]$. This is because any quantity m with the dimension of mass enters the binary’s orbit evolution as a timescale Gm/c^3 , and this timescale is redshifted. Thus, the redshift and mass of a binary black hole system are “tangled”, greatly complicating the mapping of the universe’s black hole mass distribution. The degeneracy between mass and redshift must be broken or else we cannot tell the difference between a system with mass $5 \times 10^4 M_\odot$ at $z = 1$ and a system with mass $2 \times 10^4 M_\odot$ at $z = 4$.

One way to break this degeneracy would be to associate an electromagnetic event with the coalescence. If that event had clear emission or absorption lines, one could directly read z and thus learn the system’s mass. In many cases, *LISA* will be able to measure the luminosity distance D of a source with good precision. A measurement that gives both the luminosity distance and redshift could be used to provide additional information about parameters such as the Hub-

* E-mail: hughes@itp.ucsb.edu

ble constant and the cosmological constant (Cutler 1998; Marković 1993; Wang & Taylor 1997).

It is likely that many more mergers will be measured with gravitational waves than are seen electromagnetically. Even if there is an electromagnetic signature to the coalescence, it might be missed because of effects such as beaming or absorption. Fortunately, cosmological parameters are now known well enough that we can, with good accuracy, invert the luminosity distance as a function of redshift, $D(z)$, to find the redshift as a function of luminosity distance, $z(D)$. Knowledge of the cosmological parameters allows us to break the mass-redshift degeneracy using gravitational-wave measurements alone, making it possible to untangle the mergers and map the population of massive black holes.

In this paper, we examine how well the mass-redshift degeneracy can be broken in practice. Our eventual goal is to understand how well *LISA* can measure the distribution of black hole masses as a function of redshift. Thus we will focus on how well *LISA* can measure the mass of binary black hole systems at cosmological distances, and on how well the luminosity distance and redshift can be determined.

It is worth noting at this point that the masses and luminosity distance influence the gravitational waveform in very different ways. The masses impact the binary’s dynamics, particularly the orbital frequency and inspiral rate, and thus determine the waveform’s phase evolution. One measures the masses by tracking the phase and fitting to a template. If the template’s phase maintains coherence with the signal for a large number of wave cycles, the phase — and hence the masses — can be measured quite accurately. The luminosity distance, by contrast, simply sets the overall amplitude of the wave.

Several mass parameters can be measured with gravitational waves. The early inspiral portion of the waveform (when the holes are well-separated, distinct bodies) depends most strongly on the “chirp mass”, $\mathcal{M} = (m_1 m_2)^{3/5} / (m_1 + m_2)^{1/5} = \mu^{3/5} M^{2/5}$ (where μ is the binary’s reduced mass, and M its total mass). Measuring the inspiral measures \mathcal{M} . The inspiral also depends (although rather more weakly) on the binary’s reduced mass, $\mu = m_1 m_2 / (m_1 + m_2)$. The reduced mass is not measured as precisely as the chirp mass, but is often determined well enough to be useful. The last waves to be measured from the system’s coalescence will be the “ringdown” waves, emitted as the merged system relaxes to a quiescent Kerr black hole. These waves depend only on the final state’s mass and spin, and thus directly provide the mass M_f of the final merged remnant.

As mentioned above, the major effect of the luminosity distance is to set the amplitude of the two gravitational-wave polarizations, h_+ and h_\times . These amplitudes also depend upon the chirp mass, the binary’s sky position, and its orientation. The chirp mass is determined very precisely when the wave’s phase is measured. All that remains to get the luminosity distance is to measure the sky position and orientation. These parameters are extracted by taking advantage of *LISA*’s orbital motion: as the spacecraft orbit the sun, the gravitational waveform is modulated due to the changing aspect of the source with respect to the instrument, and due to the detector’s changing antenna pattern. These modulations depend upon, and thus encode, the sky position and binary orientation. This makes it possible to measure

the luminosity distance to the source, in some cases with a precision $\delta D/D \sim 1\%$.

The luminosity distance $D(z)$ is then inverted to give the source’s redshift, $z(D)$. If the relevant cosmological parameters (fraction of closure density in matter Ω_M , cosmological constant Λ , and Hubble constant H_0) were known with perfect accuracy, then the redshift would be determined about as well as the luminosity distance: $\delta z/z \simeq \delta D/D$. In fact, each of the cosmological parameters is presently known to about 10% (Wang, Tegmark, & Zaldarriaga 2001), so it turns out that the redshift can at best be measured with about 15% precision. As future cosmological measurements pin down the universe’s geometry more precisely, the inversion will become more precise. By the time *LISA* flies (c. 2010) it is likely that in many cases cosmological uncertainties will not be the major source of error in determining the redshift of a binary black hole coalescence.

To estimate how well *LISA* will be able to untangle binary black hole mergers, we choose a range of system masses and randomly populate the sky with binaries having these masses, located at redshifts $1 \leq z \leq 9$. For simplicity, we focus on equal mass binaries, $m_1 = m_2$. We also randomly distribute the binaries’ merger time within an assumed 3 year *LISA* mission. We then use a maximum likelihood measurement formalism (Finn 1992; Finn & Chernoff 1993; Cutler & Flanagan 1994; Poisson & Will 1995) to estimate the precision with which each source’s redshifted masses and redshift can be measured. For each set of redshift and system masses, we produce the distribution of errors for the relevant parameters — the redshift z , and the redshifted chirp mass $(1+z)\mathcal{M}$, reduced mass $(1+z)\mu$, and final mass $(1+z)M_f$. The mass-redshift degeneracy is thus broken for these particular mass combinations.

The remainder of this paper is organized as follows: in Sec. 2, we briefly describe how *LISA* measures gravitational waves [following the discussion of Cutler (1998)], and summarize the formalism used to estimate parameter measurement accuracies. Section 3 describes our models for the gravitational waveform, the universe’s geometry, and the detector noise. Section 4 presents our main results, describing the accuracy with which the redshift and mass parameters can be measured by *LISA*. Using present uncertainties for our knowledge of the cosmological parameters, we find that in many cases *LISA* can measure the redshift of a system with 15 – 30% accuracy. The mass parameters — particularly the chirp mass — are often measured much more accurately than this, suggesting that the mass-redshift degeneracy will be broken with 15 – 30% error. It should be strongly emphasized at this point that the 15% lower limit on this error is dominated by present uncertainties in our knowledge of cosmological parameters. If instead luminosity distance errors dominate, it could be reduced to 5% or less.

At each redshift, there is a range of system masses for which the binary’s parameters are best determined. That is the range of masses in which the signal lies in *LISA*’s most sensitive frequency band. As we look out to larger redshifts, this “best mass” becomes smaller, since the cosmological redshift moves the relatively high frequency signal of the smaller binary into *LISA*’s band. This is probably a very useful trend, since younger (high z) black holes will tend to be smaller than older (low z) holes that have had more time to grow. Section 5 summarizes our major results; we also

discuss work that could improve this analysis. Throughout, we set the speed of light c and Newton’s gravitational constant G to unity. A useful conversion factor in these units is $1 M_\odot = 4.92 \times 10^{-6}$ seconds. Any mass parameter m written with a z subscript, m_z , denotes $(1+z)m$.

2 GRAVITATIONAL-WAVE MEASUREMENT AND PARAMETER EXTRACTION

The *LISA* gravitational-wave antenna (Danzmann et al. 1998) consists of three spacecraft arranged in an equilateral triangle orbiting the sun. The arms of the triangle are approximately $L = 5 \times 10^6$ km in length, and the triangle is inclined at an angle of 60° to the ecliptic. The entire triangular configuration spins as the antenna orbits the sun, rotating once during a single orbit (one year). A gravitational wave interacting with the configuration causes the length of the three arms to oscillate.

The gravitational-wave signal is reconstructed from the time-varying armlength data, $(\delta L_1, \delta L_2, \delta L_3)$. As described by Cutler (1998), *LISA* can be regarded as two gravitational-wave detectors. The armlength data can be combined to produce output equivalent to two detectors with 90° arms; these equivalent detectors are rotated 45° with respect to one another. This “equivalent detector” viewpoint works well when the radiation’s wavelength is greater than the armlength of the detector, but is not so accurate when $\lambda_{\text{GW}} \lesssim L$ — high frequency structure in the *LISA* sensitivity (Larson, Hiscock & Hellings 2000) is ignored. We will use the equivalent detector picture throughout this analysis, accordingly introducing some error¹ for $f_{\text{GW}} \gtrsim 0.06$ Hz. The sensitive band of the detector is taken to run from 10^{-4} Hz up to about 1 Hz.

Following Cutler’s notation, we will label the equivalent detectors “I” and “II”, so the data streams are $s_I(t)$ and $s_{II}(t)$. Each data stream consists of noise and (possibly) an astrophysical signal. We assume that the noises are stationary, Gaussian random processes with the same rms value, $\langle n_I(t)^2 \rangle = \langle n_{II}(t)^2 \rangle$, and that they are uncorrelated, $\langle n_I(t)n_{II}(t) \rangle = 0$. The two polarizations of the astrophysical gravitational-wave, $h_+(t)$ and $h_\times(t)$, enter the datastreams weighted by detector response functions, $F_{I,II}^+$ and $F_{I,II}^\times$:

$$s_{I,II}(t) = \frac{\sqrt{3}}{2} [F_{I,II}^+(t)h_+(t) + F_{I,II}^\times(t)h_\times(t)] + n_{I,II}(t). \quad (1)$$

(The factor $\sqrt{3}/2$ enters when the outputs of the real interferometers with arms at 60° are converted to the datastream of the effective interferometers, with 90° arms.) The response functions $F_{I,II}^{\pm,\times}(t)$ depend on the source’s orientation and position on the sky relative to the detector. Because any astrophysical signal will be at fixed position in the barycenter frame of the solar system, the detector’s motion induces modulations in the signal’s phase and amplitude. The response functions are written as functions of time to illustrate this orbital-motion-induced modulation. See Cutler (1998) for further discussion and details.

The gravitational waveform from a particular black hole

binary depends upon parameters θ which describe the system and its evolution. (The symbol θ stands for a vector whose components θ^a are the distance to the system, the masses of the black holes, their spins, the binary’s position on the sky, etc.) Following Finn (1992), the probability that a signal with parameters θ is present in the data streams $s_I(t)$ and $s_{II}(t)$ is given by

$$p(\theta|s_I, s_{II}) = p^{(0)}(\theta) \exp\left\{-\frac{(H_I(\theta) - s_I|H_I(\theta) - s_I) + (H_{II}(\theta) - s_{II}|H_{II}(\theta) - s_{II})}{2}\right\}. \quad (2)$$

In this equation, the inner product $(a|b)$ is

$$(a|b) = 4 \text{Re} \int_0^\infty df \frac{\tilde{a}^*(f)\tilde{b}(f)}{S_h(f)}, \quad (3)$$

where $S_h(f)$ is the spectral density of noise in the detector (discussed further in Sec. 3), the superscript * denotes complex conjugation, and $\tilde{a}(f)$ is the Fourier transform of $a(t)$:

$$\tilde{a}(f) = \int_{-\infty}^\infty dt e^{2\pi i f t} a(t). \quad (4)$$

The functions $H_{I,II}(t; \theta)$ are the gravitational waveforms measured in detectors I and II, including the motion-induced modulation:

$$H_{I,II}(t; \theta) = \frac{\sqrt{3}}{2} [F_{I,II}^+(t)h_+(t; \theta) + F_{I,II}^\times(t)h_\times(t; \theta)]. \quad (5)$$

For further discussion, see Cutler (1998). The function $p^{(0)}(\theta)$ is the prior probability distribution for the parameters θ . It encapsulates all information about the system’s parameters known before measurement [e.g., for each black hole, the spin magnitude $|\vec{S}|$ must be less than or equal to m^2 ; see Poisson & Will (1995)].

The source parameters are estimated by finding the parameters $\hat{\theta}$ that maximize $p(\theta|s_I, s_{II})$; these are the “most likely” parameters. Operationally, this is done using *matched filtering*: a bank of model waveforms (“templates”) that cover a range of parameters is assembled beforehand, and the datastreams (s_I, s_{II}) are cross-correlated with filters constructed from the templates. The parameters of the binary are estimated as those of the template with the largest cross-correlation (i.e., the template that “matches” the data). See Cutler & Flanagan (1994), Balasubrahmanian et al. (1996), and Owen (1996) for details. The template which maximizes the probability distribution (2) also gives the largest value for the signal-to-noise ratio (SNR) ρ :

$$\rho = \sqrt{\rho_I^2 + \rho_{II}^2}, \quad \rho_{I,II}^2 = (H_{I,II}(\theta)|H_{I,II}(\theta)). \quad (6)$$

We next estimate the errors in the measured parameters by expanding the probability distribution function $p(\theta|s_I, s_{II})$ about $\theta = \hat{\theta}$. To do so, we expand the inner product: denoting $\xi_{I,II}(\theta) = (H_{I,II}(\theta) - s_{I,II}|H_{I,II}(\theta) - s_{I,II})$ (Poisson & Will 1995), we have

$$\xi_{I,II}(\theta) = \xi_{I,II}(\hat{\theta}) + \frac{1}{2} \partial_a \partial_b \xi_{I,II}(\hat{\theta}) \delta\theta^a \delta\theta^b. \quad (7)$$

Here, ∂_a means partial differentiation with respect to the parameter θ^a . In the limit of large SNR (Finn 1992), $\partial_a \partial_b \xi_{I,II}/2 = (\partial_a H_{I,II}|\partial_b H_{I,II})$, so the probability distribution becomes

¹ We expect this error to be unimportant, since the luminosity distance and redshift are determined from the inspiral signal, which largely accumulates at lower frequencies.

$$p(\boldsymbol{\theta}|s_I, s_{II}) = p^0(\boldsymbol{\theta}) \exp \left[-\frac{1}{2} \Gamma_{ab} \delta\theta^a \delta\theta^b \right], \quad (8)$$

where

$$\Gamma_{ab} \equiv (\partial_a H_I | \partial_b H_I) + (\partial_a H_{II} | \partial_b H_{II}) \quad (9)$$

is the Fisher information matrix. The variance-covariance matrix Σ^{ab} is the inverse of this:

$$\Sigma^{ab} = \langle \delta\theta^a \delta\theta^b \rangle = (\Gamma^{-1})^{ab}. \quad (10)$$

The angle brackets denote an average over the probability distribution. Thus, the diagonal components, $\Sigma^{aa} = \langle (\delta\theta^a)^2 \rangle$, are the expected squared errors in the parameters θ^a . Off-diagonal components describe correlations between parameters. It is useful to introduce the correlation coefficient

$$c^{ab} = \frac{\Sigma^{ab}}{\sqrt{\Sigma^{aa}\Sigma^{bb}}}. \quad (11)$$

This coefficient lies between -1 and 1 .

Equation (10) will be the workhorse of this analysis. It will be used, along with models for the binary black hole coalescence waveform and the *LISA* noise spectrum, in order to estimate how well *LISA* will be able to measure binary parameters, particularly the luminosity distance and the system's masses.

3 MODEL AND ASSUMPTIONS

Following Flanagan & Hughes (1998), we will describe the coalescence of the black hole binary in terms of three epochs: a slow *inspiral*, in which the black holes spiral towards one another driven by adiabatic gravitational-wave emission; a far more violent and dynamical *merger*, in which the individual black holes plunge towards one another and merge into a single body; and a final *ringdown*, when the merged remnant becomes well-described as a distorted Kerr black hole.

This characterization is rather crude. In particular, the interface between “inspiral” and “merger” is not very clear cut when the members of the binary are of comparable mass. For our purposes, this characterization is useful because parameterized waveforms exist that describe the inspiral and ringdown waves, and can thus be used to study how well we will be able to determine the masses and redshifts of binary black hole coalescences. At present, the merger regime cannot be included, since its characteristics have not yet been modeled for astrophysically interesting coalescences. Numerical (Baker et al. 2001; Pfeiffer, Teukolsky, & Cook 2000; Brandt et al. 2000; Grandclément, Gourgoulhon, & Bonazzola 2001) and analytic (Buonanno & Damour 2000; Damour, Jaranowski, & Schaefer 2000; Damour 2001) work in this field is very active, and hopefully will provide useful insight into the nature of the merger and the transition from inspiral to merger by the time that *LISA* begins to make observations.

3.1 Inspiral waveform

The inspiral waveform used here is based on the post-Newtonian expansion of general relativity [see, e.g., Blanchet, Iyer, Will, & Wiseman (1996) and references

therein]. We will use waveforms computed to second-post-Newtonian (2PN) order [i.e., $(v^2/c^2)^2$ beyond the leading quadrupole result]. A very useful summary of the 2PN waveform is given in Poisson & Will (1995). It depends on seven parameters: the luminosity distance to the source $D(z)$; a coalescence time t_c ; a coalescence phase ϕ_c ; the redshifted chirp mass \mathcal{M}_z ; the redshifted reduced mass μ_z ; a spin-orbit parameter β ; and a spin-spin parameter σ .

The coalescence time and phase are essentially constants of integration, specifying the time and orbital phase of a binary at the end of inspiral. They are not physically interesting, but nonetheless must be fit for in a measurement, and thus influence the accuracy with which other parameters are measured. The chirp mass $\mathcal{M} = (m_1 m_2)^{3/5} / (m_1 + m_2)^{1/5}$ is the combination of masses that most strongly influences the gravitational-wave driven inspiral. As we shall see, this parameter tends to be measured to very high precision. The reduced mass $\mu = m_1 m_2 / (m_1 + m_2)$ gives the next most important contribution to the inspiral rate. In principle, if one measures \mathcal{M} and μ , one can solve for the individual masses of the holes in the binary [though it may turn out that μ is not determined well enough for this to work well in practice (Cutler & Flanagan 1994)]. The spin-orbit parameter β describes couplings between the spins of the black holes and the orbital angular momentum vector. It is given by

$$\beta = \frac{1}{12} \sum_{i=1}^2 [113(m_i/M)^2 + 75\mu/M] \hat{L} \cdot \vec{S}_i / m_i^2, \quad (12)$$

where $M = m_1 + m_2$, and \hat{L} is the unit vector along the orbital angular momentum. The spin-spin parameter σ likewise describes couplings between the two spins, and is given by

$$\sigma = \frac{\mu}{48M(m_1^2 m_2^2)} [721(\hat{L} \cdot \vec{S}_1)(\hat{L} \cdot \vec{S}_2) - 247(\vec{S}_1 \cdot \vec{S}_2)]. \quad (13)$$

Spin-spin and spin-orbit interactions lead to complicated precessional motions in the binary's orbit, which in turn modulate the waveform (Apostolatos et al. 1994). These modulations may provide additional information about the binary's spins and thereby reduce the effect of correlations between various parameters. However, including the effect of these modulations is rather difficult. We neglect the precession-induced modulation of the waveform in this analysis.

In the barycenter frame of reference, the two polarizations of the gravitational waveform described by these parameters is written (in the frequency domain)

$$\begin{aligned} \tilde{h}_+(f) &= \frac{\mathcal{A}}{D(z)} [1 + (\hat{L} \cdot \hat{n})^2] f^{-7/6} \exp[i\Psi(f)], \\ \tilde{h}_\times(f) &= -\frac{2\mathcal{A}}{D(z)} (\hat{L} \cdot \hat{n}) f^{-7/6} \exp[i\Psi(f)]. \end{aligned} \quad (14)$$

Here, \hat{n} is the direction vector pointing from the center of the barycenter frame (i.e., the Sun) to the system being measured. The amplitude is

$$\mathcal{A} = \sqrt{\frac{5}{96\pi}} \pi^{-2/3} \mathcal{M}_z^{5/6}, \quad (15)$$

and $\Psi(f)$ is a rather complicated function of t_c , ϕ_c , \mathcal{M} , μ , β , and σ ; see Poisson & Will (1995), Eq. (3.6).

This post-Newtonian description of \mathcal{A} and $\Psi(f)$ is more

properly called the *restricted* post-Newtonian approximation. The “full” post-Newtonian approximated waveform includes contributions from several (in principle, all) harmonics of the binary’s orbital motion (Cutler & Flanagan 1994):

$$h(t) = \text{Re} [h_1 e^{i\Phi(t)} + h_2 e^{2i\Phi(t)} + h_3 e^{3i\Phi(t)} + \dots] . \quad (16)$$

Here, $\Phi(t)$ is the time domain orbital phase. Each amplitude h_i itself is described by a post-Newtonian expansion; the results rapidly get quite complicated [cf. Will & Wiseman (1996), Eqs. (6.10) and (6.11)]. Not surprisingly, the strongest harmonic is h_2 , associated with the quadrupole moment of the source. In the restricted post-Newtonian approximation, we ignore the other harmonic contributions to the waveform. Further, we ignore all but the leading “Newtonian” order contributions to that harmonic’s amplitude. High-order post-Newtonian information is used to describe the binary’s dynamics and hence to compute the phase Φ . The Fourier transform of this restricted post-Newtonian time domain signal then gives the frequency domain waveform (14).

The location vector \hat{n} is given by the sky position coordinates of the binary, $(\bar{\mu}_S, \bar{\phi}_S)$ (where $\bar{\mu} \equiv \cos \theta$). Likewise, the binary orientation vector \hat{L} can be described using coordinates $(\bar{\mu}_L, \bar{\phi}_L)$. As *LISA* orbits the sun, the coordinates as seen by *LISA* continuously change, modulating the waveform’s amplitude and phase. Simultaneously, the detector is “rolling”, changing the profile of the arms as they “look” at a source, further modulating the waveform. For details of how this modulation works and an elegant way to build it into the waveform, see Cutler (1998). These modulations make it possible to determine the sky position of the binary to within a solid angle $\delta\Omega_S = 2\pi\delta\bar{\mu}_S\delta\bar{\phi}_S[1 - |c^{\bar{\mu}_S\bar{\phi}_S}|]$, and the orientation of the binary to within $\delta\Omega_L = 2\pi\delta\bar{\mu}_L\delta\bar{\phi}_L[1 - |c^{\bar{\mu}_L\bar{\phi}_L}|]$. If the duration of a particular measurement is too short, these angles are determined very poorly — the waveform is not modulated enough. This can severely affect the measurement of other parameters, particularly the luminosity distance. Note that the amplitudes (h_1, h_2, h_3, \dots) defined schematically in Eq. (16) each depends upon these angles in a different manner. By ignoring all but h_2 , the restricted post-Newtonian approximation throws away information that, in principle, could be used to improve gravitational-wave measurement accuracy. This is a natural point for an improved follow up to this analysis, as will be discussed further in Sec. 5.

We terminate the inspiral when the binary’s members are separated by a distance $6M$; this very roughly corresponds to the point at which the post-Newtonian expansion ceases to be accurate. The gravitational-wave frequency at this point is

$$\begin{aligned} f_{\text{gw}}(r = 6M) &= \frac{2f_{\text{orb}}(r = 6M)}{(1+z)} \\ &= \frac{2\Omega_{\text{orb}}(r = 6M)}{2\pi(1+z)} \\ &= \frac{1}{(1+z)\pi} \sqrt{\frac{M}{(6M)^3}} \\ &= \frac{6^{-3/2}}{\pi M_z} \\ &\simeq 0.04 \text{ Hz} \left(\frac{10^5 M_\odot}{M_z} \right) . \end{aligned} \quad (17)$$

The total number of inspiral parameters is eleven: the four position and orientation coordinates, the distance to the source, the constants of integration t_c and ϕ_c , and four combinations of the binary’s masses, spins, and orbital angular momentum. In Sec. 4, we determine the accuracy with which these parameters can be measured for a wide variety of interesting systems using the parameter measurement formalism discussed in Sec. 2, particularly Eq. (10). Note that we confine our discussion to the masses, the luminosity distance, and the redshift, since our primary interest is to understand what *LISA* can say about mapping the black hole mass distribution. In the course of this analysis we also fit for and estimate the errors on all the other parameters discussed in this section.

3.2 Ringdown waveform

In some cases, the waves from the final ringdown will be measurable as well. These waves are emitted as the system settles down to the stationary Kerr black hole solution. They are of relatively high frequency, so a coalescence with a very interesting inspiral may have a ringdown that is entirely lost in high frequency noise. Likewise, some systems have inspirals that are overwhelmed by low frequency noise, but emit ringdown waves right in the band of maximum sensitivity.

Weak distortions of Kerr black holes can be decomposed into spheroidal modes, with spherical-harmonic-like indices l and m (Leaver 1985). Each mode oscillates with a unique frequency f_{lm} and damping time τ_{lm} , generating gravitational waves whose form is a damped sinusoid. The frequency and damping time depend only on the mass and spin of the black hole. Measuring ringdown waves thus measures the mass and spin of the coalesced system. This provides additional information about the black hole mass distribution. It can also be combined with the chirp mass \mathcal{M} and reduced mass μ measured during the inspiral to infer the initial masses (m_1, m_2) of the binary’s members. (Because a fraction of the system’s mass is radiated away during the merger and ringdown, some systematic error is necessarily introduced when mass determined from the ringdown is combined with masses determined from the inspiral.)

The ringing waves emitted at the endpoint of binary coalescence will presumably be dominated by the $l = m = 2$ mode. This is a bar-like mode that propagates about the equator in the same sense as the hole’s spin. It is likely to dominate at late times because the coalescing system has a shape that nearly mimics an $l = m = 2$ distortion (so that it should be preferentially excited), and also because this mode is more long-lived than any other. A more detailed understanding of the merger epoch is needed to better assess the likely mixture of modes at the end of coalescence.

A good fit to the frequency $f_{22} \equiv f_{\text{ring}}$ and quality factor $Q \equiv \pi f_{\text{ring}} \tau$ is (Echeverria 1989)

$$f_{\text{ring}} = \frac{1}{2\pi M_z} [1 - 0.63(1-a)^{3/10}] , \quad (18)$$

$$Q = 2(1-a)^{-9/20} , \quad (19)$$

where $a = |\vec{S}|/M^2$ is the dimensionless Kerr spin parameter. A merged remnant with mass $10^5 M_\odot$ at $z = 1$ would emit ringdown waves somewhere in the band from $f = 0.06$ Hz ($a = 0$) to $f = 0.16$ Hz ($a = 1$). The ringdown frequency is always quite a bit higher than inspiral frequencies.

As mentioned above, the time domain gravitational waveform for the ringdown waves are damped sinusoids. They can be written

$$\begin{aligned} h_+(t) &= \mathcal{A}_+ \exp(-\pi f_{\text{ring}} t / Q) \cos(2\pi f_{\text{ring}} t + \varphi), \\ h_\times(t) &= \mathcal{A}_\times \exp(-\pi f_{\text{ring}} t / Q) \sin(2\pi f_{\text{ring}} t + \varphi). \end{aligned} \quad (20)$$

It is not easy to estimate the polarization amplitudes $\mathcal{A}_{+, \times}$; they will depend upon the detailed evolution of the merger epoch, as well as variables such as the orientation of the final merged remnant. A reasonable hypothesis is that their ratio follows the ratio of the inspiral polarization amplitudes:

$$\begin{aligned} \mathcal{A}_+ &= \mathcal{A}_{\text{ring}} [1 + (\hat{L} \cdot \hat{n})^2], \\ \mathcal{A}_\times &= -2\mathcal{A}_{\text{ring}} (\hat{L} \cdot \hat{n}). \end{aligned} \quad (21)$$

We set the overall amplitude $\mathcal{A}_{\text{ring}}$ by requiring that the ringdown radiate some fraction ϵ of the system's total mass [see Fryer, Holz, & Hughes (2001), Sec. 2.5]. The result is

$$\mathcal{A}_{\text{ring}} = \frac{1}{D(z)} \sqrt{\frac{5\epsilon M_z}{4\pi f_{\text{ring}} Q}}. \quad (22)$$

It seems likely that ϵ will vary rather strongly depending upon the constituents of the binary, particularly the black holes' spins and spin orientations. For concreteness, we will use $\epsilon = 1\%$ in all calculations. This is in accord with the fraction of system mass radiated in recent numerical simulations [see, for example, Baker et al. (2001) and references therein]. The phase φ essentially tells us the configuration of the merged remnant when the $l = m = 2$ mode dominates its dynamics. We will take it to be randomly distributed over mergers.

Whereas the inspiral waveform may be measured by *LISA* over the course of several months or years, the ringdown for any source considered here will last no more than a few hours (and in many cases, only a few minutes). This can be seen by using Eqs. (18) and (19) with $\tau = Q/\pi f_{\text{ring}}$. The motion-induced modulation of the ringdown waveform may therefore be ignored. The ringdown provides no information about the binary's location on the sky — the only characteristics of the binary we are likely to learn from the ringdown are the mass and spin of the remnant hole.

Because the ringdown waves are fairly narrow in frequency space, we may make some useful approximations when computing the expected SNR from a ringdown measurement. Suppose the ringdown begins at time T_{ring} . Define $H_{I,II}(t) = \sqrt{3}[F_{I,II}^+(T_{\text{ring}})h_+(t - T_{\text{ring}}) + F_{I,II}^\times(T_{\text{ring}})h_\times(t - T_{\text{ring}})]/2$ (since we ignore detector motion, the response functions are only evaluated at $t = T_{\text{ring}}$). Then, we have

$$\begin{aligned} \rho_{I,II}^2 &= 4 \int_0^\infty df \frac{|\tilde{H}_{I,II}(f)|^2}{S_h(f)} \\ &= 2 \int_{-\infty}^\infty df \frac{|\tilde{H}_{I,II}(f)|^2}{S_h(|f|)} \\ &\simeq \frac{2}{S_h(f_{\text{ring}})} \int_{-\infty}^\infty df |\tilde{H}_{I,II}(f)|^2 \\ &\simeq \frac{2}{S_h(f_{\text{ring}})} \int_{-\infty}^\infty dt H_{I,II}(t)^2 \\ &\simeq \frac{2}{S_h(f_{\text{ring}})} \int_{T_{\text{ring}}}^\infty dt H_{I,II}(t)^2 \end{aligned} \quad (23)$$

On the third line, we have used the fact that most of the

signal power is at $f = f_{\text{ring}}$ to pull the noise out of the integral, on the fourth line we have used Parseval's theorem to go from a frequency domain to a time domain integral, and on the fifth line we have used the fact that ringdown waves by definition are zero before T_{ring} . This final integral is simple to evaluate using Eq. (20).

We could now apply the full parameter estimation formalism discussed in Sec. 2 to see how well the mass M and spin a of the remnant black hole can be determined. Such an analysis has in fact already been performed (Finn 1992). Because the detector motion has no important impact, Finn's results carry over directly to this analysis. In particular, the final mass is determined to an accuracy

$$\frac{\delta M_{f,z}}{M_{f,z}} = \frac{\mathcal{F}(a)}{\rho} \simeq \frac{2}{\rho} = \frac{2}{\sqrt{\rho_I^2 + \rho_{II}^2}}. \quad (24)$$

The function $\mathcal{F}(a)$ slowly varies from roughly 2.5 for a Schwarzschild black hole to 0.5 for an extreme Kerr hole. Since the goal of this analysis is a simple estimate, and also since the initial conditions for ringing waves from coalescences are not well known, we consider approximating $\mathcal{F}(a) \simeq 2$ to be as accurate as is warranted.

3.3 Cosmological model

The cosmological parameters enter this analysis through the need to convert between redshift and luminosity distance. We will assume a flat cosmology, with matter and cosmological constant contributions to the total density given by $\Omega_\Lambda = 0.65$ and $\Omega_M = 1 - \Omega_\Lambda = 0.35$. These choices are in accord with recent observational evidence (e.g., Netterfield et al. 2001). The luminosity distance to a source at redshift z is given by [Hogg (1999) and references therein]

$$D(z) = \frac{(1+z)c}{H_0} \int_0^z \frac{dz'}{E(z')}, \quad (25)$$

where

$$E(z) = \sqrt{\Omega_M(1+z)^3 + \Omega_\Lambda}. \quad (26)$$

The Hubble constant $H_0 = 100 h_0$ km/(Mpc s); we assume $h_0 = 0.65$ (Wang, Tegmark, & Zaldarriaga 2001).

This expression is very easy to invert numerically; we do so with a simple bisection, obtaining $z(D)$. For a particular gravitational-wave measurement, we get D with some error δD . This error, and also errors in the cosmological parameters Ω_Λ and h_0 , mean that z is measured to a precision δz :

$$\delta z = \frac{\partial z}{\partial D} \left[\delta D^2 + \left(\frac{\partial D}{\partial \Omega_\Lambda} \right)^2 \delta \Omega_\Lambda^2 + \left(\frac{\partial D}{\partial h_0} \right)^2 \delta h_0^2 \right]^{1/2}, \quad (27)$$

where

$$\begin{aligned} \frac{\partial z}{\partial D} &= \left(\frac{\partial D}{\partial z} \right)^{-1}, \\ \frac{\partial D}{\partial z} &= \frac{c}{H_0} \left[\frac{(1+z)}{E(z)} + \int_0^z \frac{dz'}{E(z')} \right], \\ \frac{\partial D}{\partial \Omega_\Lambda} &= \frac{(1+z)c}{2H_0} \int_0^z dz' \frac{[(1+z')^3 - 1]}{E(z')^3}, \\ \frac{\partial D}{\partial h_0} &= -\frac{D(z)}{h_0}. \end{aligned} \quad (28)$$

Note that $\delta\Omega_M$ is not included since we have assumed that the universe is precisely flat, and therefore $\delta\Omega_M = -\delta\Omega_\Lambda$. Following the discussion in Wang, Tegmark, & Zaldarriaga (2001), we will put $\delta\Omega_\Lambda = 0.1$ and $\delta h_0 = 0.1$. When $\delta D/D \ll 10\%$, δz is dominated by $\delta\Omega_\Lambda$ and δh_0 ; in these cases, it typically turns out that $\delta z/z \simeq 15\%$. We will also look at redshift measurement accuracy assuming that $\delta\Omega_\Lambda = 0 = \delta h_0$; this demonstrates how well the redshift could be measured in principle if the universe's geometry were known perfectly.

This assumed cosmology is adequate for the purposes of this paper. As our knowledge of the universe's geometry improves, this prescription can be readily generalized (for example, if the “dark energy” turns out to have an equation of state other than that of a cosmological constant).

3.4 Detector noise

Finally, we need a model for the noise in the *LISA* detector to proceed. As discussed in Sec. 2, we assume that the noise in each of the effective detectors is a stationary, Gaussian random process. We also assume that their noises are uncorrelated. As discussed by Cutler (1998), one can combine the data streams in such a way that this second assumption is true by construction.

The detector noise is characterized by the spectral density $S_h(f)$. This quantity is the Fourier transform of the autocorrelation of the time domain noise:

$$\begin{aligned} S_h(f) &= 2 \int_{-\infty}^{\infty} d\tau C_n(\tau) e^{2\pi i f \tau}, \\ C_n(\tau) &= \langle n(t)n(t+\tau) \rangle, \end{aligned} \quad (29)$$

where angle brackets denote ensemble averaging. We assume that the spectral density is the same for each of the effective detectors.

LISA's datastream will include instrumental noise intrinsic to the detector, and confusion noise arising primarily from the large number of gravitational wave producing white dwarf binaries in the galaxy. Especially at low frequencies, one cannot resolve these binaries individually — for a mission lasting $T \sim$ several 10^7 seconds, there could be as many as 10^3 binaries contributing power in a single frequency bin $\delta f \sim 1/T$ (Cutler 1998). The unresolved white dwarf binaries constitute a stochastic background that, from the perspective of measuring black hole binary waves, is a source of noise.

A good fit (Phinney, private communication) to the projected instrumental noise for *LISA* (Folkner 1998) is given by

$$\begin{aligned} S_h^{\text{inst}}(f) &= \left\{ s_1 [1 + f/(0.01 \text{ Hz})] + s_2/f^2 \right. \\ &\quad \left. + s_3/f^{5/2} + s_4(10^{-4} \text{ Hz}/f)^{20} \right\}^2, \end{aligned} \quad (30)$$

where

$$\begin{aligned} s_1 &= 4 \times 10^{-21} \text{ Hz}^{-1/2}, \\ s_2 &= 3 \times 10^{-26} \text{ Hz}^{3/2}, \\ s_3 &= 5 \times 10^{-28} \text{ Hz}^2, \\ s_4 &= 1 \times 10^{-16} \text{ Hz}^{-1/2}. \end{aligned} \quad (31)$$

Notice that this noise shoots up very rapidly at frequencies

less than 10^{-4} Hz. In fact, *LISA* could have good sensitivity at lower frequencies than this [cf. Fig. 5 of Larson, Hiscock, & Hellings (2000)]. The very low-frequency sensitivity will be limited by *LISA*'s ability to maintain “drag-free” motion on long timescales (that is, motion driven solely by gravity, without interference from external forces due to, for example, the solar wind). In cutting off *LISA*'s sensitivity at 10^{-4} Hz, we assume that drag-free behavior will be difficult to maintain on timescales longer than about 3 hours.

The galactic confusion noise is well described by

$$\begin{aligned} S_h^{\text{gal}}(f) &= 5 \times 10^{-44} \text{ Hz}^{-1} \left(\frac{1 \text{ Hz}}{f} \right)^{7/3} \\ &\quad \times [1 - \exp(-\delta f dN/df)]. \end{aligned} \quad (32)$$

The factor in square brackets gives the fraction of frequency bins near f that have a contribution from galactic white dwarf binaries. This fraction decreases with increasing frequency — the population of white dwarf binaries thins out in frequency space at high f . This is because the inspiral rate df/dt grows with f , so a population that is initially clustered near some frequency spreads out as it evolves. In this equation, we put $\delta f = 3/T$, where T is the duration of the *LISA* mission, and the factor 3 roughly accounts for the smearing of a white dwarf binary's signal due to detector motion. The function

$$\frac{dN}{df} = 2 \times 10^{-3} \text{ Hz}^{-1} \left(\frac{1 \text{ Hz}}{f} \right)^{11/3} \quad (33)$$

is the number of white dwarf binaries per unit gravitational-wave frequency. The fit (32) was provided by Phinney (Phinney, private communication); the prefactor 5×10^{-44} and the value of dN/df correspond closely to the results presented in Webbink & Han (1998).

At high enough frequencies, there will be on average fewer than one white dwarf binary per bin. The confusion noise goes from a smooth continuum to a series of non-confused lines. For galactic binaries, these lines should be strong enough that they can be fit and subtracted from the data stream, reducing the overall noise. A simple estimate of the resulting noise (Phinney, private communication) is

$$\begin{aligned} S_h^{\text{inst+gal}}(f) &= \min \left[S_h^{\text{inst}}(f) / \exp(-\delta f dN/df), \right. \\ &\quad \left. S_h^{\text{inst}}(f) + 5 \times 10^{-44} \text{ Hz}^{-1} (1 \text{ Hz}/f)^{7/3} \right]. \end{aligned} \quad (34)$$

The factor $\exp(-\delta f dN/df)$ is the fraction of empty bins. For the total *LISA* noise, we take (34) plus a contribution from extragalactic binaries (Folkner 1998):

$$S_h^{\text{ex. gal}}(f) = 1.1 \times 10^{-46} \text{ Hz}^{-1} \left(\frac{1 \text{ Hz}}{f} \right)^{7/3}. \quad (35)$$

Finally, it should be noted that Phinney has recently re-examined the issue of confusion limited backgrounds in very general terms (Phinney 2001a), and will soon produce a paper pointing out some overlooked sources of confusion noise (Phinney 2001b). These noises are not included in this analysis, but could be very easily. Their main effect will be to augment the low-frequency noise, thus reducing the signal-to-noise ratio. The accuracy with which parameters

can be measured will be reduced as well, but very likely that reduction will nearly scale with the reduction in SNR.

4 RESULTS

To determine how well *LISA* will be able to measure masses and redshift, we have performed a large number of Monte Carlo simulations of binary black hole coalescence measurement. We choose binary masses and a redshift, and then randomly distribute 100 such binaries over sky position and orientation. We also randomly distribute the binary members' spins, and the magnitude of the final merged hole's spin. (Of course, the final spin should be found by conserving the initial spin and orbital angular momentum of the system, less that which is lost to radiation. The details of this are complicated and depend to some degree on poorly understood physics. For the purpose of estimating how well the final system mass is determined, randomly choosing the final spin should be fine.) Finally, we assume that the *LISA* mission lasts three years, and we uniformly distribute the coalescence time of the binary during that time. As a consequence, the total observation time may vary quite a bit among inspirals in a particular run, which can have a large impact on parameter determination. The routine `ran2()` (Press et al. 1992) was used to generate random numbers.

The binaries chosen were placed at $z = 1, 3, 5, 7, 9$, and had masses $m_1 = m_2 = 10^{3,4,5,6,7} M_\odot$. For each redshift and mass, we develop the distribution of parameter determination errors. Two examples of such distributions are illustrated in Figures 1 and 4. Figure 1 shows the distribution of errors in z , \mathcal{M}_z , μ_z , and $M_{f,z}$ expected for measurements of a binary with $m_1 = m_2 = 10^5 M_\odot$ at $z = 1$. This is a case where most parameters are measured rather well. Note in particular the extreme precision with which the redshifted chirp mass is determined: the distribution peaks at $\delta\mathcal{M}_z/\mathcal{M}_z \sim 1.5 \times 10^{-4}$. The chirp mass is measured so precisely because it most strongly determines the inspiral rate, and hence has the greatest impact on the gravitational wave phase evolution. The reduced mass also impacts the inspiral, but not as strongly, and hence is measured with less precision: the peak in the distribution is at $\delta\mu_z/\mu_z \sim 2.5 \times 10^{-2}$. Finally, note that the redshift errors peak at $\delta z/z \sim 15\%$. This is the value expected when the redshift error is dominated by the present uncertainty in our knowledge of cosmological parameters. The luminosity distance is actually determined far better than this, indicating that improved knowledge of cosmological parameters will greatly reduce errors in the redshift. This is illustrated in Fig. 2. The top panel shows the distribution in luminosity distance errors, and the bottom panel illustrates the redshift error that would be achieved if we knew the cosmological parameters exactly. Comparing the two panels shows that $\delta z/z \simeq \delta D/D$ when the cosmological parameters are known accurately. Both of these distributions peak near 1% relative error, and are largely confined to less than 10% error. The rule of thumb “ $\delta z/z \simeq \delta D/D$ when $\delta(\text{cosmology}) = 0$ ” holds more or less independent of redshift. As cosmological parameters become better determined, our ability to determine the redshift (and thus the masses) of coalescing binary black holes will be greatly improved.

Table 1 is a somewhat massaged representation of the

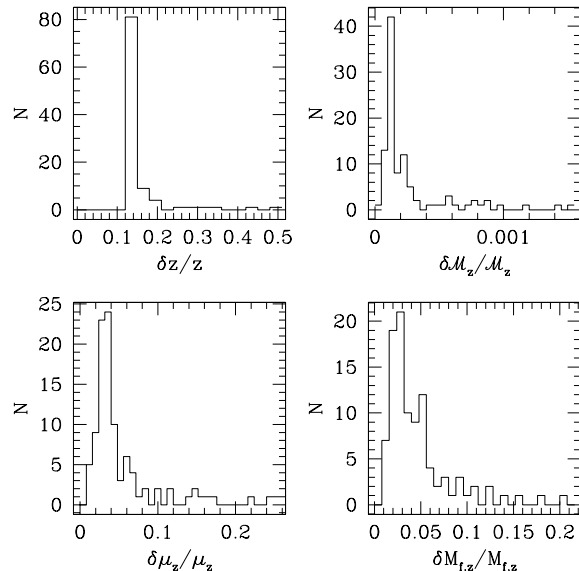


Figure 1. Distribution of errors in z , \mathcal{M}_z , μ_z , and $M_{f,z}$ for *LISA* measurement of a binary with $m_1 = m_2 = 10^5 M_\odot$ at $z = 1$. The typical inspiral SNR is about 1000; the ringdown SNR is around 65. This mass is nearly optimal at this redshift for determining the binary’s parameters. The error in z is dominated by errors in the cosmological parameters; the luminosity distance is actually determined quite precisely for this source (cf. Fig. 2).

covariance matrix Σ^{ab} for a typical inspiral in this distribution — diagonal components are actually the mean error $\langle(\delta\theta^a)^2\rangle^{1/2} = \sqrt{\Sigma^{aa}}$, off-diagonal components are the correlation coefficient c^{ab} defined in Eq. (11). Note the strong correlations between the luminosity distance and the position and orientation angles. These parameters are rather strongly entangled since they set the amplitude of the measured waveform: the angles through the detector response functions F^+ and F^\times and the ratio of the wave’s polarizations; the luminosity distance through the overall amplitude \mathcal{A} [cf. Eq. (15)]. In order to make a good measurement of the luminosity distance, we must determine the binary’s sky position and orientation very accurately. The sky position and orientation are encoded in the modulations induced by *LISA*’s orbital motion; they are well determined when the waveform is subject to a large amount of this motion-induced modulation. Hence, luminosity distance is only well determined when the waveform is significantly modulated by the detector motion. This accounts for the rather large tails apparent in Figs. 1 and 2: though most of the distribution for $\delta D/D$ (for example) is confined to small error, some of the coalescences in the sample are measured with much larger $\delta D/D$, up to 60%. These large error measurements occur when the inspiral is shorter than usual — because we randomly distribute the merger time during *LISA*’s mission, some events occur very near the mission’s start. The position and orientation angles are poorly determined for these short inspirals, so the luminosity distance is also determined poorly.

The impact of these correlations on the accuracy with which D is measured can be assessed by imagining that the binary’s sky position is measured with zero error. This is a

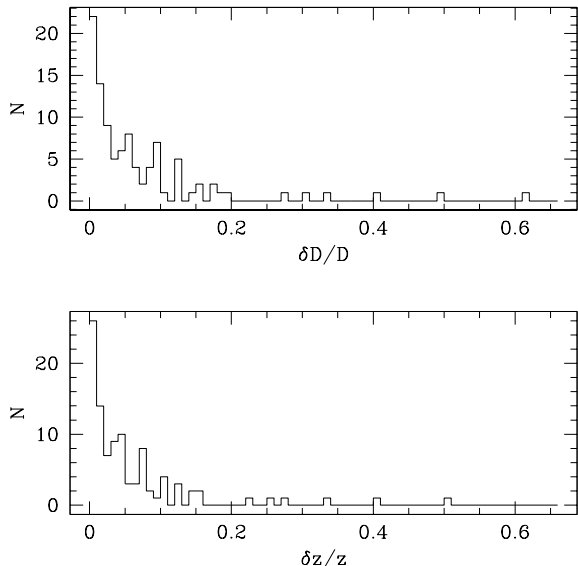


Figure 2. The top panel shows the distribution of error in luminosity distance D for *LISA* measurement of binaries with $m_1 = m_2 = 10^5 M_\odot$ at $z = 1$; the bottom panel shows how well the redshift could be measured if cosmological parameters were known perfectly. In both cases, the peak of the distribution is at a relative error near 1%. This indicates that in many cases the mass-redshift degeneracy will be broken with very good precision when cosmological parameters are better determined. Note, though, the very large tail in the distribution, extending out to relative error of about 60%. The distance to the source is poorly determined when a source’s sky position is poorly determined. This typically happens if the observation time is short — the merger occurs near the beginning of *LISA*’s mission.

reasonable description of what might be achieved by coordinated electromagnetic and gravitational-wave measurements of binary coalescence — for instance, if the merger is accompanied by a gamma or x-ray flare. The electromagnetic measurement will likely determine the merger’s sky position much more accurately than can be done with gravitational waves. Figure 3 compares how well D is measured when the sky position is known precisely to the case of sky position determined from the gravitational waves. Knowledge of the binary’s sky position has an enormous impact, improving the accuracy with which D is measured by about an order of magnitude.

Note that Table 1 also shows strong correlations among the mass and spin parameters, \mathcal{M}_c , μ , β , and σ . This is a well-known feature of measurement with post-Newtonian templates, arising because the impact of the various parameters upon the phase evolution are not strongly different from one another. For further discussion, see Cutler & Flanagan (1994) and Poisson & Will (1996).

Figure 4 shows the distribution of measurement errors when $m_1 = m_2 = 10^4 M_\odot$ and $z = 7$. In all cases, the distributions peak at larger error values than when $m_1 = m_2 = 10^5 M_\odot$ and $z = 1$. This isn’t too surprising since these sources are much fainter and thus harder to measure. The redshift determination in particular is quite a bit worse, so that the mass-redshift degeneracy will be broken rather less accurately for these holes. Table 2 shows the pa-

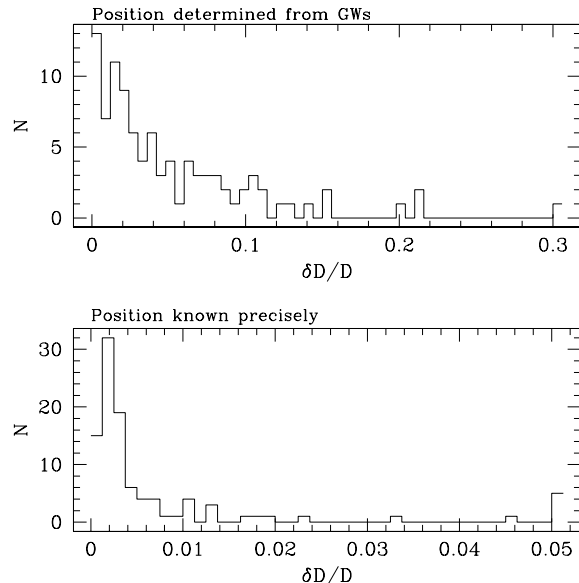


Figure 3. Comparison of measurement errors in luminosity distance for *LISA* measurement of a binary with $m_1 = m_2 = 10^5 M_\odot$ at $z = 1$. The top panel shows the error distribution when the sky position is determined using gravitational waves; the bottom panel shows the distribution assuming the sky position is measured with no error. Because of strong correlations between the luminosity distance and the sky position angles, improving the accuracy with which the position is measured has a big impact on the distance determination. In this case, D is measured with roughly an order of magnitude less error.

parameter errors and correlations for a typical coalescence in this set. Because of the signal’s weakness, the measurement errors (diagonal components of the matrix) are rather larger than in the case $z = 1$, $m_1 = m_2 = 10^5 M_\odot$. However, the correlations (off-diagonal components) are not much different. This is typical: correlations between inspiral parameters do not depend strongly on signal-to-noise ratio, though the inspiral time can have a big effect.

Rather than show distribution histograms for all the remaining cases that we examined, we summarize their contents in Tables 3 – 7. These tables give the “most likely” error values — the errors found at the peaks of the measurement distribution. The reader should bear in mind that the distributions from which these values were taken also have long, high-error tails, as in the Figures.

Several interesting features can be seen across the tables. Only Table 3 includes data for the merger of holes with $m_1 = m_2 = 10^7 M_\odot$. At redshifts higher than $z = 1$, the inspiral signal from such binaries is radiated at frequencies entirely below 10^{-4} Hz, out of *LISA*’s band. Indeed, even at $z = 1$ this binary barely radiates in band, lasting less than 2 hours before merger. The signal is so short that little inspiral phase accumulates, so D , \mathcal{M}_z , and μ_z are determined very poorly. The ringdown, by contrast, is quite strong, so $M_{f,z}$ is measured with very good accuracy.

The tables show that, in general, measurement accuracy degrades with increasing redshift. This isn’t surprising since such sources are fainter. However, at each redshift, there are some sources and parameters that can be measured with at least moderate precision. At low redshift, there is a fairly

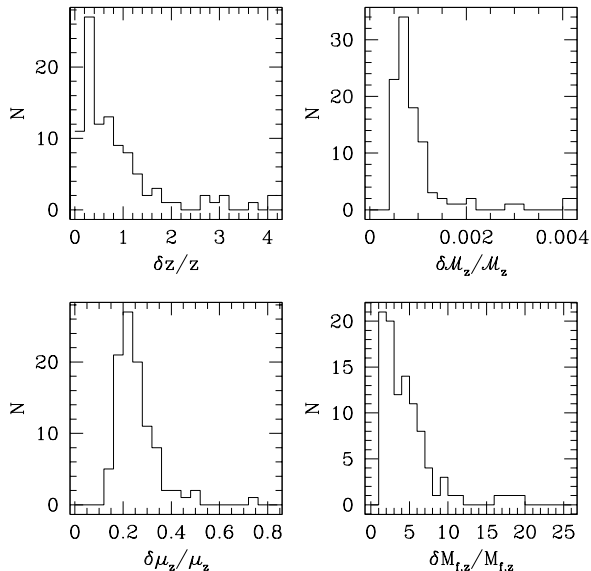


Figure 4. Distribution of errors in z , \mathcal{M}_z , μ_z , and $M_{f,z}$ for *LISA* measurement of a binary with $m_1 = m_2 = 10^4 M_\odot$ at $z = 7$. The typical inspiral SNR is about 45; the ringdown SNR is around 0.7. Because of the weak ringdown waves, the final mass is rather poorly determined. In this case, measurement error and cosmological parameter error contribute to the redshift error about equally. Setting the cosmological parameter errors to zero in this case does not have a large effect.

broad range of masses in which at least two of the masses (\mathcal{M}_z , μ_z , $M_{f,z}$) can be determined with good precision, and in some cases all three are well measured. Out to $z = 5$, there are cases for which $\delta D/D < \delta z/z$, indicating that in those cases the redshift distribution is skewed high because of the present error in h_0 and Ω_Λ . Setting the cosmological parameter error to zero, we find $\delta z/z \simeq \delta D/D$, as expected. Improved knowledge of cosmological parameters will have a big impact on measurement in those cases. At redshifts $z > 5$, δz becomes dominated by error in D — improved knowledge of h_0 and Ω_Λ will not have much effect.

Finally, note that the tables confirm the trend discussed above that D (and hence z) is not well determined for very short measurement times: if the inspiral does not last “long enough”, the motion-induced modulation of the waveform is not sufficient to determine the source’s sky position and orientation very accurately. As a consequence, D is poorly determined. A rough necessary condition to measure D well seems to be that the *LISA* constellation must move through a radian or so of its orbit. This is *not*, however, a sufficient condition — D can be determined poorly from long inspirals if the signal is too weak.

In all cases except for the largest masses, the best determined parameter is the redshifted chirp mass. It is often measured with precision $\delta \mathcal{M}_z/\mathcal{M}_z \lesssim 0.1\%$ or better, even from sources with $z \sim 9$. *LISA*’s ability to break the mass-redshift degeneracy for the chirp mass will therefore be limited by redshift error: we will measure the *actual* chirp mass of distant coalescences to within 15 – 30% assuming present cosmological parameters, and perhaps as well as 5 – 30% when *LISA* actually flies. The reduced mass is often mea-

sured with a precision of about 10% or better, and so provides useful additional information. The final mass of the system is only determined from more massive systems, since the ringdown waves are relatively high frequency. In those cases, it can be measured with accuracy $\delta M_{f,z}/M_{f,z} \lesssim 5\%$.

5 SUMMARY AND CONCLUSION

By combining gravitational-wave measurements with information about cosmological parameters, *LISA* will be able to measure the redshift of coalescing binaries with moderate precision (relative error of 15 – 30% using present uncertainties in cosmological parameters, perhaps 5 – 30% by the time that *LISA* flies). The redshifted chirp mass is typically measured far more accurately than this, and in many cases, either the binary’s reduced mass or the final mass of the remnant black hole produced when the binary merges can be measured with a precision of 5 – 20%. This precision will allow *LISA* to untangle mass and redshift, making it possible to track the merger history of massive black holes in the universe.

These measurements work best for signals whose frequency range lies in *LISA*’s band of maximum sensitivity. From Tables 3 – 7, we see that the best measurement sensitivities are for systems that have $M_z \sim 10^5 M_\odot$ or so. This isn’t too surprising: recall that inspiral ends when the bodies are separated by a distance $r \sim 6M$, and that the gravitational-wave frequency at that point is

$$f_{\text{GW}} \simeq 0.04 \text{ Hz} \left(\frac{10^5 M_\odot}{M_z} \right) \quad (36)$$

[cf. Eq. (17)]. This frequency is right about where *LISA*’s sensitivity begins to degrade due to high frequency noise. When $M_z \sim 10^5 M_\odot$ most of the inspiral signal accumulates in a band where *LISA* has very good sensitivity. A good rule of thumb seems to be that *LISA* will measure at least two of the redshifted mass combinations \mathcal{M}_z , μ_z , and $M_{f,z}$ with good precision when the total redshifted system mass is within a factor of ten to twenty of $10^5 M_\odot$. Even outside that range, at least one mass (either the chirp mass or the final mass) can be measured well.

To measure the redshift precisely, we first must determine the luminosity distance. This correlates most strongly with the amount of time over which the inspiral signal is measured. Very short inspirals do not experience enough detector-motion-induced modulation of the gravitational waveform to pin down a source’s location on the sky very accurately, and as a consequence the luminosity distance can be poorly determined. This is the reason the largest systems in our sample have such poor precision in D and z : they enter *LISA*’s band already very close to merging, and quickly evolve to merger. The distance is determined well when *LISA* moves through at least a radian or so of its orbit, corresponding to at least 2 months of observation.

This analysis is essentially just a first cut, proof-of-principle demonstration of how cosmological information and gravitational-wave measurements can be combined to study the merger history of massive black holes. We have made several simplifying assumptions that, if lifted, may modify some of our conclusions. One example is our use

of the restricted post-Newtonian approximation. In analyzing the inspiral, we have thrown out all but the strongest, quadrupole harmonic of the binary's orbit. Other harmonics contribute as well, though, and should be measurable by *LISA*. Because the amplitude of each harmonic depends on source parameters (particularly the binary's inclination angle) in a different way, measuring multiple harmonics could greatly improve the distance determination by breaking degeneracies between D and the source orientation angles² (apparent in the large correlation coefficients shown in Tables 1 and 2).

A better understanding of the merger epoch could also improve parameter estimation. The merger waves are, by definition, all of the radiation emitted at frequencies between the end of inspiral and the ringdown. In some cases, these waves are likely to be very strong and interesting, particularly if the black holes in the binary are rapidly rotating (Flanagan & Hughes 1998; Price & Whelan 2001). They will probably be rather short duration (perhaps 10-20 cycles at $f \sim 0.05$ Hz when $M_z \sim 10^5 M_\odot$), and so provide essentially no information about the source location and distance. But they could give some information about the binary's masses and spins, which could break some degeneracies and improve the accuracy of parameters measured during the inspiral.

We have used a rather simple, smooth power-law fit to *LISA*'s projected instrumental noise curve. This is adequate for first-cut estimates, but is in principle wrong, particularly at high frequencies when the radiation wavelength is shorter than *LISA*'s arms. Following the analysis of Larson, Hiscock, & Hellings (2000) it is straightforward to describe *LISA*'s response to a gravitational-wave more precisely. In practice, this will require a moderate amount of effort, particularly since *LISA*'s response function and noise curve turn out to depend upon a source's sky position. This response will put additional position-dependent structure into a particular measurement, which could be used to further improve positional accuracy. This merits some detailed investigation.

A source of systematic error that has been neglected in this analysis is gravitational lensing. Gravitational waves are lensed exactly as electromagnetic radiation is lensed, and this will impact the accuracy with which parameters are measured. Since *LISA* will be watching binary coalescence events out to large redshift, we expect that weak lensing will be common; if the number of mergers is large, there may also be some strongly lensed mergers. Lensing will have little or no effect on the determination of the redshifted masses, since they are measured from the signal's phase evolution, but will impact the wave's amplitude. A lens with large skew could also change the relative magnitude of the $+$ and \times polarizations. The source's orientation and sky position could thus be determined incorrectly, which may skew the measurement of D , and thence the determination of z (Marković 1993).

Finally, it would be very useful to tie these estimates more closely to hierarchical structure formation scenarios (see, e.g., Menou, Haiman, & Narayanan 2001), and to understand how much *LISA* could impact such models. It would also be valuable to understand the rate of mergers at large redshift [in analogy with the analysis of Menou,

Haiman, & Narayanan (2001), which estimates rates out to $z \sim 5$]. If this rate turns out to be *too* high, binary black hole mergers might actually be a confusion limited source of noise (Phinney 2001a) rather than an opportunity to study structure formation.

I thank Ron Hellings, Daniel Holz, Shane Larson, and Sterl Phinney for many useful discussions. I am also grateful to the astrophysics and relativity group of Cornell University and the Center for Gravitational Physics and Geometry at Penn State, where a portion of the code used in this analysis was written. This research was supported by NSF Grant PHY-9907949.

REFERENCES

- Apostolatos, T., Cutler, C., Sussman, G. J., Thorne, K. S. 1994, Phys. Rev. D 49 6274
- Baker, J., Brüggmann, B., Campanelli, M., Lousto, C. and Takahashi, R. 2001, Phys. Rev. D, submitted; gr-qc/0102037
- Balasubrahmanian, R., Sathyaprakash, B. S., and Dhurandar, S. V. 1996, Phys. Rev. D 53, 3033; Phys. Rev. D 54, 1860(E)
- Blanchet, L., Iyer, B. R., Will, C. M., and Wiseman, A. G. 1996, Class. Quantum Grav. 13, 575
- Brandt, S. et al. 2000, Phys. Rev. Lett. 85, 5496
- Buonanno, A. and Damour, T. 2000, Phys. Rev. D 62, 064015
- Cutler, C. 1998, Phys. Rev. D 57, 7089
- Cutler, C. and Flanagan, E. E. 1994, Phys. Rev. D 49, 2658
- Danzmann, K. et al. 1998, *LISA — Laser Interferometer Space Antenna, Pre-Phase A Report*, Max-Planck-Institut für Quantenoptik, Report MPQ 233 (1998)
- Damour, T. 2001, Phys. Rev. D, submitted; gr-qc/0103018
- Damour, T., Jaranowski, P., and Schaefer, G. 2000, Phys. Rev. D 62, 084011
- Echeverria, F. 1989, Phys. Rev. D 40, 3194
- Fan, X. et al. (the SDSS collaboration), AJ 120, 1167
- Finn, L. S. 1992, Phys. Rev. D 46, 5236
- Finn, L. S. and Chernoff, D. F. 1993, Phys. Rev. D 47, 2198
- Flanagan, E. E. and Hughes, S. A. 1998, Phys. Rev. D 57, 4535
- Folkner, W. M. in Folkner, W. M. 1998, editor, *Laser Interferometer Space Antenna, Second International LISA Symposium on the Detection and Observation of Gravitational Waves in Space*, AIP Conference Proceedings, Vol. 456, p 11
- Fryer, C. L., Holz, D. E., and Hughes, S. A. 2001, ApJSupp, in press; astro-ph/0106113
- Gnedin, O. 2001, to appear in the Proceedings of the Third International LISA Symposium; astro-ph/0108070
- Grandclément, P., Gourgoulhon, E., and Bonazzola, S. 2001, Phys. Rev. D, submitted; gr-qc/0106016
- Haehnel, M. G., in Folkner, W. M. 1998, editor, *Laser Interferometer Space Antenna, Second International LISA Symposium on the Detection and Observation of Gravitational Waves in Space*, AIP Conference Proceedings, Vol. 456, p 45
- Hogg, D. W. 1999, "Distance measures in cosmology", astro-ph/9905116
- Larson, S. L., Hiscock, W. A., and Hellings, R. W. 2000, Phys. Rev. D 62, 062001
- Leaver, E. W. 1985, Proc. R. Soc. Lond. A402, 285
- Marković, D. M. 1993, Phys. Rev. D 48, 4738
- Menou, K., Haiman, Z. and Narayanan, V. K. 2001, ApJ, submitted; astro-ph/0101196
- Milosavljević, M. and Merritt, D. 2001, ApJ, submitted; astro-ph/0103350
- Netterfield, C. B. et al. 2001, ApJ, submitted; astro-ph/0104460
- Owen, B. J. 1996, Phys. Rev. D 53, 6749
- Pfeiffer, H. P., Teukolsky, S. A., and Cook, G. B. 2000, Phys. Rev. D 62, 104018

² The author is very grateful to Ron Hellings for bringing this point to his attention.

- Phinney, E. S., private communication
- Phinney, E. S. 2001a, Mon. Not. R. Astron. Soc., submitted; astro-ph/0108028
- Phinney, E. S. 2001b, in preparation
- Poisson, E. and Will, C. M. 1995, Phys. Rev. D 52, 848
- Press, W. H., Teukolsky, S. A., Vetterline, W. T., and Flannery, B. P. 1992, *Numerical Recipes* (New York: Cambridge University Press)
- Price, R. H. and Whelan, J. T., gr-qc/0107029
- Stern, D., Spinrad, H., Eisenhardt, P., Bunker, A., Dawson, S., Stanford, A., and Elston, R. 2000, ApJ 120, 1607
- Thorne, K. S., in Kolb, E. W. and Peccei, R. 1995, editors, *Particle and Nuclear Astrophysics and Cosmology in the Next Millennium: Proceedings of the 1994 Snowmass Summer Study* (World Scientific, Singapore); gr-qc/9506086
- Haehnelt, M. G., in Folkner, W. M. 1998, editor, *Laser Interferometer Space Antenna, Second International LISA Symposium on the Detection and Observation of Gravitational Waves in Space*, AIP Conference Proceedings, Vol. 456, p 45
- Wang, Y. and Taylor, E. L. 1997, Phys. Rev. D 56, 724
- Wang, X., Tegmark, T. and Zaldarriaga, M. 2001, Phys. Rev. D, submitted; astro-ph/0105091
- Webbink, R. F. and Han, Z., in W. M. in Folkner, W. M. 1998, editor, *Laser Interferometer Space Antenna, Second International LISA Symposium on the Detection and Observation of Gravitational Waves in Space*, AIP Conference Proceedings, Vol. 456, p 61
- Will, C. M. and Wiseman, A. G. 1996, Phys. Rev. D 54, 4813
- Zheng, W. et al. (the SDSS collaboration) 2000, AJ 120, 1607

This paper has been typeset from a $\text{\TeX}/\text{\LaTeX}$ file prepared by the author.

Table 1. Measurement accuracy and correlations for coalescences at $z = 1$ with $m_1 = m_2 = 10^5 M_\odot$. Diagonal elements in this matrix are the mean error expected in the parameter; off-diagonal elements are the correlation coefficient c^{ab} . Elements containing \cdot can be found by symmetry. The errors in ϕ_L , ϕ_S , and ϕ_c are in radians; those in t_c are in units of 10^4 seconds. All other entries are dimensionless.

| | $\ln D$ | μ_L | μ_S | ϕ_L | ϕ_S | t_c | ϕ_c | $\ln \mathcal{M}_z$ | $\ln \mu_z$ | β | σ |
|---------------------|---------|---------|---------|----------|----------|---------|----------|---------------------|-------------|---------|----------|
| $\ln D$ | 0.0095 | 0.8969 | 0.8258 | 0.6692 | 0.8185 | -0.0532 | 0.3224 | 0.1608 | -0.2196 | 0.2182 | -0.2076 |
| μ_L | \cdot | 0.0114 | 0.8215 | 0.2972 | 0.8881 | -0.1140 | 0.2273 | -0.0143 | -0.0625 | 0.0502 | -0.1048 |
| μ_S | \cdot | \cdot | 0.0006 | 0.4474 | 0.7591 | -0.1786 | 0.2526 | 0.0823 | -0.1402 | 0.1353 | -0.1483 |
| ϕ_L | \cdot | \cdot | \cdot | 0.0362 | 0.3280 | 0.0777 | 0.3351 | 0.3884 | -0.3883 | 0.4063 | -0.2879 |
| ϕ_S | \cdot | \cdot | \cdot | \cdot | 0.0051 | -0.0802 | 0.2074 | 0.0067 | -0.0703 | 0.0612 | -0.0100 |
| t_c | \cdot | \cdot | \cdot | \cdot | \cdot | 0.0002 | 0.8837 | 0.7522 | -0.8287 | 0.7980 | -0.9189 |
| ϕ_c | \cdot | \cdot | \cdot | \cdot | \cdot | \cdot | 0.7179 | 0.8691 | -0.9473 | 0.9247 | -0.9918 |
| $\ln \mathcal{M}_z$ | \cdot | \cdot | \cdot | \cdot | \cdot | \cdot | \cdot | 0.0001 | -0.9798 | 0.9904 | -0.8828 |
| $\ln \mu_z$ | \cdot | \cdot | \cdot | \cdot | \cdot | \cdot | \cdot | \cdot | 0.0334 | -0.9976 | 0.9556 |
| β | \cdot | \cdot | \cdot | \cdot | \cdot | \cdot | \cdot | \cdot | \cdot | 0.4171 | -0.9331 |
| σ | \cdot | \cdot | \cdot | \cdot | \cdot | \cdot | \cdot | \cdot | \cdot | \cdot | 0.3251 |

Table 2. Measurement accuracy and correlations for coalescences at $z = 7$ with $m_1 = m_2 = 10^4 M_\odot$.

| | $\ln D$ | μ_L | μ_S | ϕ_L | ϕ_S | t_c | ϕ_c | $\ln \mathcal{M}_c$ | $\ln \mu_z$ | β | σ |
|---------------------|---------|---------|---------|----------|----------|---------|----------|---------------------|-------------|---------|----------|
| $\ln D$ | 0.2036 | -0.2030 | 0.8774 | -0.6732 | -0.6861 | -0.3873 | -0.2672 | -0.4736 | 0.3933 | -0.4331 | 0.2200 |
| μ_L | \cdot | 0.6189 | -0.5836 | -0.4715 | -0.4980 | -0.7733 | 0.0455 | 0.0608 | -0.0245 | 0.0258 | -0.0177 |
| μ_S | \cdot | \cdot | 0.3647 | -0.4104 | -0.3818 | -0.0090 | -0.2387 | -0.4250 | 0.3413 | -0.3758 | 0.1907 |
| ϕ_L | \cdot | \cdot | \cdot | 0.7262 | 0.9927 | 0.9066 | 0.2173 | 0.3933 | -0.3429 | 0.3792 | -0.1863 |
| ϕ_S | \cdot | \cdot | \cdot | \cdot | 0.4652 | 0.9261 | 0.2182 | 0.3898 | -0.3412 | 0.3771 | -0.1861 |
| t_c | \cdot | \cdot | \cdot | \cdot | \cdot | 0.0083 | 0.1932 | 0.2900 | -0.2768 | 0.2992 | -0.1778 |
| ϕ_c | \cdot | \cdot | \cdot | \cdot | \cdot | \cdot | 4.0390 | 0.9008 | -0.9562 | 0.9354 | -0.9960 |
| $\ln \mathcal{M}_z$ | \cdot | \cdot | \cdot | \cdot | \cdot | \cdot | \cdot | 0.0005 | -0.9848 | 0.9931 | -0.9012 |
| $\ln \mu_z$ | \cdot | \cdot | \cdot | \cdot | \cdot | \cdot | \cdot | \cdot | 0.1479 | -0.9977 | 0.9589 |
| β | \cdot | \cdot | \cdot | \cdot | \cdot | \cdot | \cdot | \cdot | \cdot | 2.1417 | -0.9373 |
| σ | \cdot | \cdot | \cdot | \cdot | \cdot | \cdot | \cdot | \cdot | \cdot | \cdot | 1.9260 |

Table 3. Summary of measurement accuracies for binary black hole coalescences at $z = 1$. The redshift error δz_1 assumes $\delta h_0 = 0.1$, $\delta \Omega_\Lambda = 0.1$; the error δz_2 assumes the cosmological parameters are known perfectly.

| $m_1 (= m_2)$ | ρ_{insp} | T_{insp} | ρ_{ring} | $\delta D/D$ | $\delta z_1/z$ | $\delta z_2/z$ | $\delta \mathcal{M}_z/\mathcal{M}_z$ | $\delta \mu_z/\mu_z$ | $\delta M_{f,z}/M_{f,z}$ |
|----------------|----------------------|-------------------|----------------------|--------------|----------------|----------------|--------------------------------------|----------------------|--------------------------|
| $10^3 M_\odot$ | 20 | 575 days | 10^{-3} | 0.08 | 0.15 | 0.05 | 5×10^{-5} | 0.05 | 2500 |
| $10^4 M_\odot$ | 150 | 550 days | 0.25 | 0.05 | 0.15 | 0.04 | 5×10^{-5} | 0.03 | 10 |
| $10^5 M_\odot$ | 1000 | 430 days | 60 | 0.02 | 0.15 | 0.02 | 1×10^{-4} | 0.04 | 0.03 |
| $10^6 M_\odot$ | 200 | 15 days | 3500 | 0.2 | 0.2 | 0.2 | 5×10^{-3} | 0.5 | 5×10^{-4} |
| $10^7 M_\odot$ | 40 | 100 minutes | 612 | 70 | 70 | 70 | 150 | 300 | 4×10^{-3} |

Table 4. Summary of measurement accuracies for binary black hole coalescences at $z = 3$.

| $m_1 (= m_2)$ | ρ_{insp} | T_{insp} | ρ_{ring} | $\delta D/D$ | $\delta z_1/z$ | $\delta z_2/z$ | $\delta \mathcal{M}_z/\mathcal{M}_z$ | $\delta \mu_z/\mu_z$ | $\delta M_{f,z}/M_{f,z}$ |
|----------------|----------------------|-------------------|----------------------|--------------|----------------|----------------|--------------------------------------|----------------------|--------------------------|
| $10^3 M_\odot$ | 10 | 575 days | 10^{-3} | 0.2 | 0.2 | 0.2 | 1×10^{-4} | 0.08 | 1000 |
| $10^4 M_\odot$ | 75 | 530 days | 0.35 | 0.1 | 0.15 | 0.1 | 5×10^{-4} | 0.1 | 5 |
| $10^5 M_\odot$ | 400 | 200 days | 85 | 0.1 | 0.15 | 0.1 | 1×10^{-3} | 0.3 | 0.02 |
| $10^6 M_\odot$ | 70 | 5 days | 1300 | 0.8 | 0.8 | 0.8 | 1.5×10^{-2} | 0.6 | 1×10^{-3} |

Table 5. Summary of measurement accuracies for binary black hole coalescences at $z = 5$.

| $m_1 (= m_2)$ | ρ_{insp} | T_{insp} | ρ_{ring} | $\delta D/D$ | $\delta z_1/z$ | $\delta z_2/z$ | $\delta \mathcal{M}_z/\mathcal{M}_z$ | $\delta \mu_z/\mu_z$ | $\delta M_{f,z}/M_{f,z}$ |
|----------------|----------------------|-------------------|----------------------|--------------|----------------|----------------|--------------------------------------|----------------------|--------------------------|
| $10^3 M_\odot$ | 9 | 540 days | 2×10^{-3} | 0.25 | 0.3 | 0.25 | 2×10^{-4} | 0.1 | 1000 |
| $10^4 M_\odot$ | 55 | 560 days | 0.6 | 0.2 | 0.2 | 0.2 | 2×10^{-4} | 0.2 | 4 |
| $10^5 M_\odot$ | 250 | 100 days | 100 | 0.15 | 0.2 | 0.15 | 3×10^{-3} | 0.5 | 0.02 |
| $10^6 M_\odot$ | 30 | 2.5 days | 350 | 2 | 2 | 2 | 0.05 | 0.6 | 0.01 |

Table 6. Summary of measurement accuracies for binary black hole coalescences at $z = 7$.

| $m_1(=m_2)$ | ρ_{insp} | T_{insp} | ρ_{ring} | $\delta D/D$ | $\delta z_1/z$ | $\delta z_2/z$ | $\delta \mathcal{M}_z/\mathcal{M}_z$ | $\delta \mu_z/\mu_z$ | $\delta M_{f,z}/M_{f,z}$ |
|----------------|----------------------|-------------------|----------------------|--------------|----------------|----------------|--------------------------------------|----------------------|--------------------------|
| $10^3 M_\odot$ | 9 | 540 days | 3×10^{-3} | 0.3 | 0.3 | 0.3 | 2.5×10^{-4} | 0.15 | 500 |
| $10^4 M_\odot$ | 46 | 560 days | 0.7 | 0.25 | 0.25 | 0.25 | 7×10^{-4} | 0.25 | 1.5 |
| $10^5 M_\odot$ | 150 | 65 days | 120 | 0.5 | 0.5 | 0.5 | 5×10^{-3} | 0.6 | 0.015 |
| $10^6 M_\odot$ | 24 | 1.5 days | 100 | 6 | 6 | 6 | 0.1 | 0.7 | 0.03 |

Table 7. Summary of measurement accuracies for binary black hole coalescences at $z = 9$.

| $m_1(=m_2)$ | ρ_{insp} | T_{insp} | ρ_{ring} | $\delta D/D$ | $\delta z_1/z$ | $\delta z_2/z$ | $\delta \mathcal{M}_z/\mathcal{M}_z$ | $\delta \mu_z/\mu_z$ | $\delta M_{f,z}/M_{f,z}$ |
|----------------|----------------------|-------------------|----------------------|--------------|----------------|----------------|--------------------------------------|----------------------|--------------------------|
| $10^3 M_\odot$ | 8 | 580 days | 4×10^{-3} | 0.5 | 0.5 | 0.5 | 3×10^{-4} | 0.16 | 500 |
| $10^4 M_\odot$ | 43 | 530 days | 0.9 | 0.3 | 0.3 | 0.3 | 7×10^{-4} | 0.25 | 1.5 |
| $10^5 M_\odot$ | 100 | 45 days | 130 | 1 | 1 | 1 | 7×10^{-3} | 0.6 | 0.015 |
| $10^6 M_\odot$ | 17 | 1 day | 40 | 20 | 20 | 20 | 0.6 | 1.5 | 0.05 |